Aquatic Sciences 52/2, 1990

1015-1621/90/020115-15 $ 1.50 + 0.20/0

The SOMS model and its application to Lake Neuchâtel

E. A. H. Zuur [1] and D. E. Dietrich [2]

[1] PROSPER, University of Neuchâtel, Switzerland
[2] Sandia National Laboratories, Albuquerque, New Mexico

Key words: Conservative primitive equations; general circulation model.

ABSTRACT

A three-dimensional numerical circulation model (SOMS) based on primitive equations is described. The algorithm, by which Coriolis and vertical diffusion terms are treated implicitly while mass is still conserved exactly (algebraically), is discussed in detail. The model is applied to Lake Neuchâtel (Switzerland), to determine the general circulation under influence of the most prevailing wind.

1. Introduction

Mathematical computer models are currently being used with relevant observations to assess transport and dispersion of soluble and suspendable materials in lakes and oceans, originating from various sources. The model that is described in this paper is a three dimensional numerical circulation model based on primitive equations. Originally it was developed for ocean studies at Sandia National Laboratories in Albuquerque, and is referred to as the SOMS model (Sandia Ocean Modelling System). The model has advantageous stability characteristics and the operation-count per time step is relatively small compared with other 3D methods (see Dietrich, 1987). Therefore, a high resolution of the computational grid is possible. The model is applied to Lake Neuchâtel (Switzerland), to provide a first overview of the general circulation induced by the most prevailing wind.

This paper includes a description of the SOMS model and illuminates in particular the specific predictor-corrector scheme by which the surface pressure is determined and the part of the algorithm that treats Coriolis and vertical diffusion implicitly, while mass is still exactly conserved in the algebraic sense. Further, results of applying the model to Lake Neuchâtel under barotropic conditions are presented.

2. The continuum equations

2.1 *Hypotheses and approximations*

The Navier-Stokes (N-S) equations, a set of non-linear partial differential equations, together with an equation of state, an energy equation, and appropriate boundary and initial conditions govern Newtonian fluids (see Batchelor, 1967). The special nature of the Lake problem allows certain approximations that are used to simplify the governing equations. The resulting system is integrated using a fast computer such as a CRAY-2. Scaling estimates of the terms that appear in the N-S equations justify the following approximations (Pedlosky, 1987):

- The Boussinesq approximation: density variations are neglected in the horizontal momentum and mass conservation equations, but are taken into account when they are associated with buoyancy forces (in the vertical momentum equation). Density is assumed independent of pressure and varies only with temperature.
  The hydrostatic approximation: all terms in the vertical momentum equation are neglected except the buoyancy and pressure gradient terms.
  The *f*-plane approximation: a Cartesian coordinate system attached to the earth with constant Coriolis parameter.
- The rigid lid approximation (see below).
- A relatively simple turbulence closure scheme (see below).

Two categories of water motion can be distinguished, namely the gravitational response and the non-divergent response. The gravitational response is characterized by divergent motion, with a significant ratio of potential to kinetic energy. The time-scale of this response is proportional to the length of the lake divided by the speed of the long gravity waves (the seiche period). It is in the order of minutes for Lake Neuchâtel. For the non-divergent response, however, most of the energy is kinetic and the time-scale is larger than the seiche period. The rigid lid (non-divergent) model which is applied here therefore simulates the transient, large scale circulation in the Lake.

When the equations are solved on a finite space-time domain, the molecular diffusion becomes negligible compared to turbulence effects at a scale smaller than the grid-size of this domain. Although variations at this scale are not resolved by the model, their effect on the resolved motion is important through non-linear interactions. The usual way to account for this effect is to decompose all variables into a mean value and a fluctuating value. Then, the resulting set of equations for the mean values, with the effect of the fluctuating part on the mean flow defined by additional model assumptions, has to be solved. Many levels of sophistication can be used to account for this turbulence part (Mellor and Yamada, 1982). Here, we use a rather popular and relatively simple method: the turbulence is represented in the mean flow equations by means of so-called turbulence viscosity coefficients, which are determined by a simple theoretical model (Pedlosky, 1987).

2.2 *The model equations*

The continuum equations used in SOMS are derived from the previous hypotheses and approximations. They are stated below.

The momentum equations:

$$\frac{\partial u}{\partial t} = -\frac{1}{\varrho_0}\frac{\partial p}{\partial x} + fv - \nabla\cdot(u\,\mathbf{v}) + \frac{\partial}{\partial x}\left(A_h\frac{\partial u}{\partial x}\right) + \frac{\partial}{\partial y}\left(A_h\frac{\partial u}{\partial y}\right) + \frac{\partial}{\partial z}\left(A_v\frac{\partial u}{\partial z}\right), \quad (1)$$

$$\frac{\partial v}{\partial t} = -\frac{1}{\varrho_0}\frac{\partial p}{\partial y} - fu - \nabla\cdot(v\,\mathbf{v}) + \frac{\partial}{\partial x}\left(A_h\frac{\partial v}{\partial y}\right) + \frac{\partial}{\partial y}\left(A_h\frac{\partial v}{\partial y}\right) + \frac{\partial}{\partial z}\left(A_v\frac{\partial v}{\partial z}\right). \quad (2)$$

The hydrostatic equation:

$$\frac{\partial p}{\partial z} = \varrho g\,. \quad (3)$$

The mass conservation equation:

$$\frac{\partial u}{\partial x} + \frac{\partial v}{\partial y} + \frac{\partial w}{\partial z} = 0\,. \quad (4)$$

The equation of state:

$$\varrho = \varrho_0\,(1 - \alpha T)\,. \quad (5)$$

The heat equation:

$$\frac{\partial T}{\partial t} = -\nabla\cdot(T\,\mathbf{v}) + Q(T)\,, \quad (6)$$

in which $Q(T)$ represents sources, sinks, and the diffusive redistribution of T.

The following symbols are used:

x, y, z	spatial coordinates in a left-handed Cartesian system (z-axis points downwards) $[L]$;
t	time $[T]$;
T	(in situ) temperature $[\Theta]$;
u, v, w	velocity components ($\mathbf{v} = (u, v, w)$) $[L\,T^{-1}]$;
p	pressure $[M\,L^{-1}\,T^{-2}]$;
ϱ	density (ϱ_0 is reference density) $[M\,L^{-3}]$;
g	effective gravitational acceleration $[L\,T^{-2}]$;
A_h	horizontal eddy diffusion $[L^2\,T^{-1}]$;
A_v	vertical eddy diffusion $[L^2\,T^{-1}]$;
f	Coriolis parameter $[T^{-1}]$;
α	coefficient of thermal expansion $[\Theta^{-1}]$;
∇	$= (\partial/\partial x, \partial/y, \partial/\partial z)$.

3. Numerical algorithm

The set of continuum equations stated in 2.2 applied to the lake cannot be solved analytically, therefore solutions will be sought numerically. Thus, the space-time domain has to be discretized, and the differential equations must be replaced by algebraic equations for the unknown nodal values of the computational grid.

3.1 Space and time integration

Spatial integration is performed with a finite difference method. The space domain is represented by a finite number of computational points in a 3D-Eulerian computational grid. The grid is regular, but stretched in the vertical coordinate, in order to model accurately the surface and/or bottom boundary layer (Dietrich, 1987). The computational points for different quantities, such as pressure and velocity components, are actually staggered in space (see fig. 1), corresponding to the widely used Arakawa-C grid (Arakawa and Lamp, 1977). The grid cells are considered either wholly inside or wholly outside the lake region. In the remainder subscribts and superscribts indicate spatial- and time-discretization respectively.

For all relevant time dependent quantities the leapfrog method is used in combination with the filtered leapfrog-trapezoidal scheme (FLT) to avoid the tendency of the leapfrog method to decouple solutions at alternate time steps.

In the leapfrog method, as well the time- as the space-derivatives are approximated by centered differences. Consider for convenience only the one dimensional advection equation:

$$\frac{\partial q}{\partial t} = -u\frac{\partial q}{\partial x}, \tag{7}$$

where u is the constant advection velocity. The leapfrog method is:

$$q_i^{n+1} = q_i^{n-1} - c\,(q_{i+1}^n - q_{i-1}^n), \tag{8}$$

in which $c = u\Delta t/\Delta x$ is the Courant number (Roache, 1976).

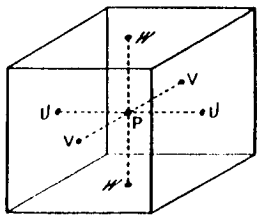

Figure 1. Arakawa-C staggered grid single control volume for pressure. The symbol P denotes the centre of the P-control volume. The symbols U, V and W denote relative positions of control volume centres for horizontal and vertical velocity components

The FLT method consists in substituting q_i^{n-1} in (8) by $(q_i^n + q_i^{n-2})/2$, which actually adds a time filter to the leapfrog method, but does not introduce spatial damping. Let us denote a weighted linear combination of q_i^{n-1} and its filtered value by:

$$\hat{q}^{n-1} = (1-\omega)\,q_i^{n-1} + \omega(q_i^n + q_i^{n-2})/2. \tag{9}$$

Combining leapfrog and FLT leads to:

$$q_i^{n+1} = \hat{q}_i^{n-1} - c\,(q_{i+1}^n - q_{i-1}^n). \tag{10}$$

This integration method is known as the filtered leap-frog-trapezoidal weighted (FLTW) scheme. A description of the properties of the FLTM method is found in Roache and Dietrich (1988).

3.2 Time step procedure

This paragraph describes the overall procedure of one time step. Two specific features of this procedure will be pointed out already: the mass conservation equation is satisfied exactly (algebraically) after every time step; Coriolis and vertical diffusion are treated implicitly for reasons to be discussed in section 3.3.

Before describing the numerical procedure, first some relations are derived from the continuum equations, and some definitions are given. From (3) and (5) it follows that:

$$p = p_s(x,y) + \varrho_0 g z - \varrho_0 g \alpha \int_0^z T(x,y,\zeta)\,d\zeta, \tag{11}$$

in which p_s is the surface pressure (p_s is different from the atmospheric pressure due to the rigid lid approximation). Define:

$$L = fv + \frac{\partial}{\partial z}\left(A_v\frac{\partial u}{\partial z}\right), \tag{12}$$

$$M = -fu + \frac{\partial}{\partial z}\left(A_v\frac{\partial v}{\partial z}\right), \tag{13}$$

$$R = g\alpha\int_0^z \frac{\partial T}{\partial x}\,d\zeta - V\cdot(u\,v) + \frac{\partial}{\partial x}\left(A_h\frac{\partial u}{\partial x}\right) + \frac{\partial}{\partial y}\left(A_h\frac{\partial u}{\partial y}\right), \tag{14}$$

$$S = g\alpha\int_0^z \frac{\partial T}{\partial y}\,d\zeta - V\cdot(v\,v) + \frac{\partial}{\partial x}\left(A_h\frac{\partial v}{\partial x}\right) + \frac{\partial}{\partial y}\left(A_h\frac{\partial v}{\partial y}\right). \tag{15}$$

(Note: L and M contain the Coriolis and vertical diffusion terms). Putting (11) to (15) into the momentum equations (1) and (2) yields:

$$\frac{\partial u}{\partial t} = -\frac{1}{\varrho_0}\frac{\partial p_s}{\partial x} + L + R, \tag{16}$$

$$\frac{\partial v}{\partial t} = -\frac{1}{\varrho_0}\frac{\partial p_s}{\partial y} + M + S. \tag{17}$$

Due to the rigid lid approximation, the vertical velocity is zero at the surface. From (4) we obtain:

$$w = \int_0^z \left(\frac{\partial u}{\partial x} + \frac{\partial v}{\partial y}\right) d\zeta. \tag{18}$$

Applying the no-slip condition at the bottom yields:

$$0 = \int_0^h \left(\frac{\partial u}{\partial x} + \frac{\partial v}{\partial y}\right) d\zeta, \tag{19}$$

in which $h = h(x, y)$ is the bottom-depth. By differentiating (16) to x, (17) to y, adding the equations and integrating the result on both sides from surface to bottom (from (19) it follows that the remaining left-hand side is zero), we obtain a 2D Poisson equation for the surface pressure:

$$\frac{\partial^2 p_s}{\partial x^2} + \frac{\partial^2 p_s}{\partial y^2} = \frac{\varrho_0}{h}\int_0^h \left(\frac{\partial L}{\partial x} + \frac{\partial R}{\partial x} + \frac{\partial M}{\partial y} + \frac{\partial S}{\partial y}\right) d\zeta. \tag{20}$$

The numerical procedure can be divided into three parts. The first part makes it possible to treat the L and M terms implicitly when the Poisson equation for the surface pressure is solved. The second part solves this Poisson equation. The third part updates the velocity components and temperature with the resulting surface pressure.

Consider the magnitudes of all time dependent quantities to be known at time $n\Delta t$. The derivation of the magnitudes at time $(n+1)\Delta t$ is described below.

First p_s^{n+1} is approximated by the known p_s^n and the "intermediate" velocity components $\tilde{u}^{n+1}$ and $\tilde{v}^{n+1}$ are calculated from the momentum equations. They serve to evaluate the L and M terms when p_s^{n+1} is calculated from the Poisson equation. They are calculated from the following set of equations:

$$\tilde{u}_{ijk}^{n+1} = \hat{u}_{ijk}^{n-1} + 2\Delta t\left[-\frac{1}{\varrho_0}\frac{\partial p_s^n}{\partial x} + L(\tilde{u}^{n+1}, \tilde{v}^{n+1}) + R^n\right]_{ijk}, \tag{21}$$

$$\tilde{v}_{ijk}^{n+1} = \hat{v}_{ijk}^{n-1} + 2\Delta t\left[-\frac{1}{\varrho_0}\frac{\partial p_s^n}{\partial y} + M(\tilde{u}^{n+1}, \tilde{v}^{n+1}) + S^n\right]_{ijk}, \tag{22}$$

in which:

$$\bar{u}^{n+1} = (\tilde{u}^{n+1} + u^n)/2, \text{ and} \tag{23}$$

$$\bar{v}^{n+1} = (\tilde{v}^{n+1} + v^n)/2. \tag{24}$$

The L and M terms are treated implicitly, which means that these terms are also a function of the unknown velocity field components at time $(n+1)\Delta t$. The system is solved with appropriate boundary conditions (see section 4), either directly or with a relaxation method.

The second part of the time step procedure solves the Poisson equation using $\tilde{u}^{n+1}$ and $\tilde{v}^{n+1}$ to determine the L and M terms. With (20) we get:

$$\left[\frac{\partial^2 p_s^{n+1}}{\partial x^2} + \frac{\partial^2 p_s^{n+1}}{\partial y^2}\right]_{ij} = \left[\frac{\varrho_0}{h}\int_0^h \left(\frac{\partial L(\bar{u}^{n+1}, \bar{v}^{n+1})}{\partial x} + \frac{\partial R^n}{\partial x} + \frac{\partial M(\bar{u}^{n+1}, \bar{v}^{n+1})}{\partial y} + \frac{\partial S^n}{\partial y}\right) d\zeta\right]_{ij}. \tag{25}$$

This set of equations is solved with the Neumann boundary condition. (The surface pressure is determined except for an additive constant, which is arbitrary, because only pressure gradients are used in the momentum equations).

Finally, the new horizontal velocity components u^{n+1} and v^{n+1} are derived from the right-hand sides of (21) and (22) by substituting p_s^n by p_s^{n+1}. The vertical velocity and the temperature are calculated from the discretized versions of (18) and (6) respectively, and $\hat{u}^n$ and $\hat{v}^n$ are calculated with (9). This completes the time step procedure.

3.3 *Numerical stability*

The finite difference scheme is such that the Coriolis terms conserve energy exactly (algebraically). Further, the new velocity-field satisfies exactly (algebraically) mass conservation equation (3). This desirable feature is also a property of the "Marker-and-Cell" method (MAC) from Harlow and Welch (1966). However, in the MAC scheme Coriolis and vertical diffusion are not treated implicitly.

Coriolis and vertical diffusion are treated implicitly in SOMS to avoid undesirable time step limits when the boundary layers are adequately resolved. Ekman layer thickness is roughly determined by scale analysis of a balance between vertical diffusion and Coriolis terms (Pedlovsky, 1984). If this thickness is adequately resolved, the smallest resolved vertical modes decay on a time scale that is small compared to the Coriolis time scale, leading to a generally undesirable time step limitation if the vertical diffusion is treated explicitly.

The main time step limiting processes are thus internal wave propagation, and horizontal advection and diffusion. Compared to internal wave terms, horizontal diffusion and advection are quite often relatively small.

4. Application of the model to Lake Neuchâtel

4.1 Description of the Lake

Lake Neuchâtel is a quasi-rectangular body of water in western Switzerland. Its surface is artificialy maintained at a mean altitude of 429 m above see-level by a dam. Its longest axis is directed SW-NE. The maximum length is 38.3 km, the average width 5.68 km, and the maximum depth 136 m. The bathymetry of the lake is "elongated bath-tub" like with a bump centered in the NE region (see fig. 2). This bump (called la Motte) is a rather steep mountain with its peak only about 10 m under the water-surface.

The dominant wind is le Vent, a SW wind, blowing along the long axis of the Lake.

More information about the morphology of the Lake, its inlets and its wind is found in Bapst (1988) and Sollberger (1974).

4.2 Simulation

The simulations performed were intended to provide a first overview of the general circulation in Lake Neuchâtel under barotropic conditions induced by the most prevailing wind.

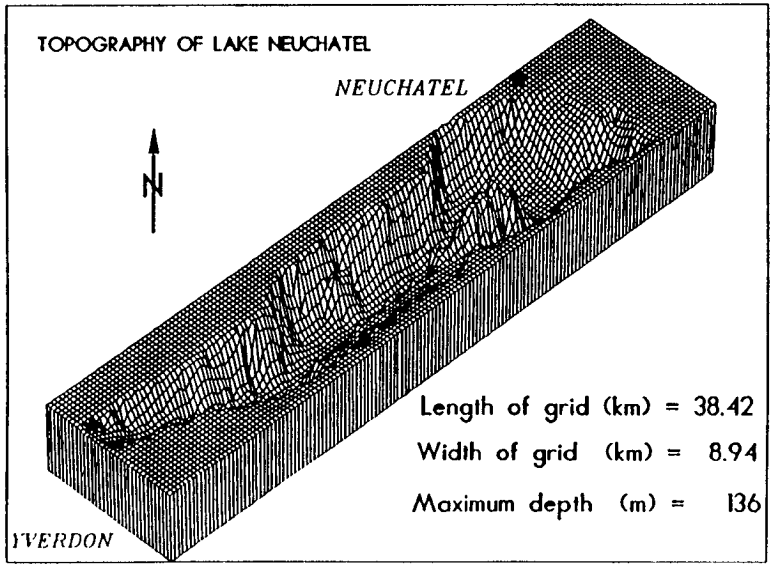

Figure 2. Topography of Lake Neuchâtel

The lake is considered to be a closed basin. So, the influence on the general circulation of rivers and small streams that enter the lake is neglected. The wind conditions are as follows. Wind is blowing from the south-west (le Vent). The wind speed remains constant the first twelve hours. Then the wind is turned off, and the model is kept running without wind-forcing for another six hours. At the start of both simulations the lake is at rest ($v = 0$).

The volume of the Lake is filled with control volumes. A horizontal plane contains 134×34 control volumes, the area of each control volume being 263×263 m^2. In the vertical direction there are 20 layers of control volumes, the thickness of each layer being defined by a vertically stretched vertical coordinate to model correctly the surface Ekman layer. The bottom Ekman layer is not resolved by the model, and therefore, instead of the no-slip condition, a shear stress law is applied at the bottom (see below).

The wind stress is related to the wind speed by a "bulk aerodynamic" formula

$$(\tau_{sx}, \tau_{sy}) = \varrho_a C_D \sqrt{(U^2 + V^2)}\,(U, V), \tag{26}$$

where ϱ_a ($= 1.225$ kg/m^3) is the air's density, $(U, V) = (7.5, 0)$ m/s is the air velocity at an elevation of 3 m above the lake-surface, and C_D ($= 0.002$) is the drag coefficient corresponding to this elevation. So, the boundary conditions for the velocity components at the surface are

$$\varrho_0 A_v \left(\frac{\partial u}{\partial z}, \frac{\partial v}{\partial z}\right) = (\tau_{sx}, \tau_{sy}), \tag{27}$$

$$w = 0. \tag{28}$$

The bottom shear stress is related to the velocity in the bottom layer according to

$$(\tau_{bx}, \tau_{by}) = \varrho_0 r \sqrt{(u_b^2 + v_b^2)}\,(u_b, v_b), \tag{29}$$

in which (u_b, v_b) is the horizontal velocity in the last layer. r ($= 0.0025$) is the drag coefficient at the bottom. The boundary conditions at the bottom are

$$\varrho_0 A_v \left(\frac{\partial u}{\partial z}, \frac{\partial v}{\partial z}\right) = (\tau_{bx}, \tau_{by}), \tag{30}$$

$$w = 0. \tag{31}$$

The horizontal turbulent viscosity coefficient is taken constant, $A_h = 10$ m^2/s. The vertical turbulent viscosity A_v is defined as (see Hutter, 1984)

$$A_v = \nu_0 + \nu_1 \sqrt{(\tau_{sx}^2 + \tau_{sy}^2)}\, e^{-z/d}, \tag{32}$$

in which $\nu_0 = 25$ cm^2/s, $\nu_1 = 100$ cm^3 s/gr, and $d = 20$ m.

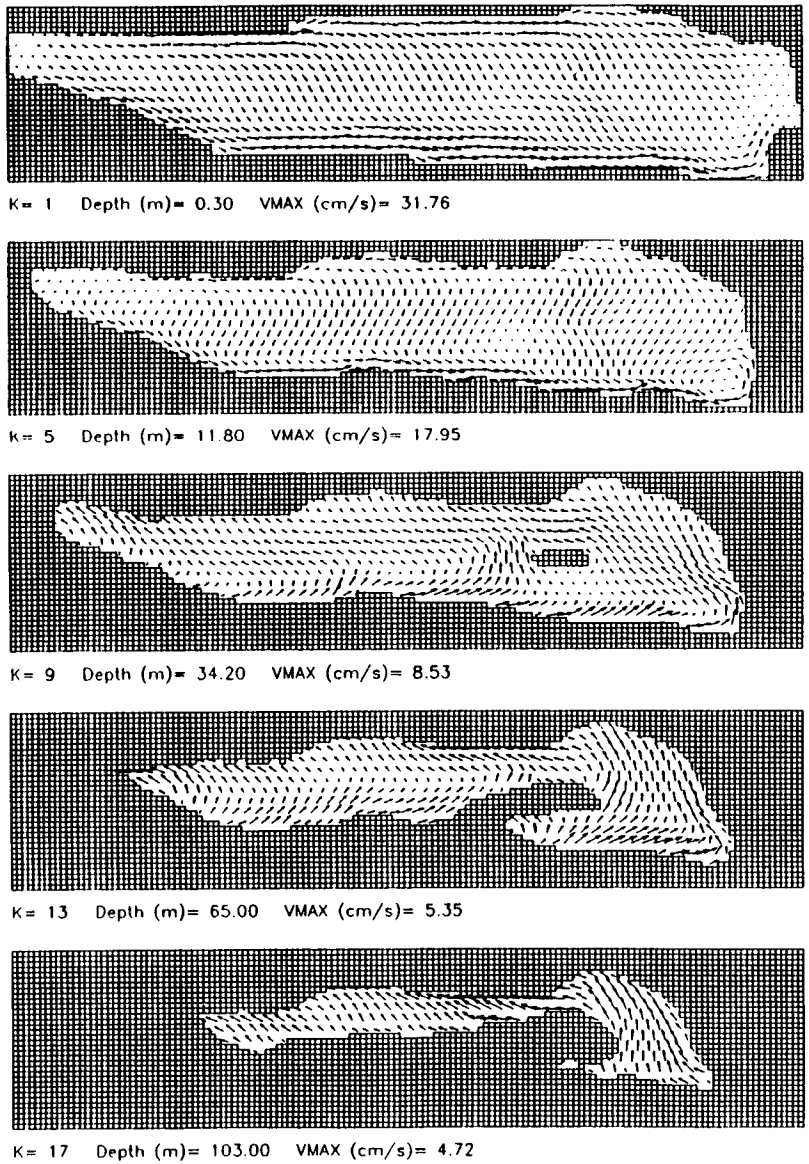

Figure 3. Horizontal velocity field at 5 depth-levels after 12 hours of wind-forcing

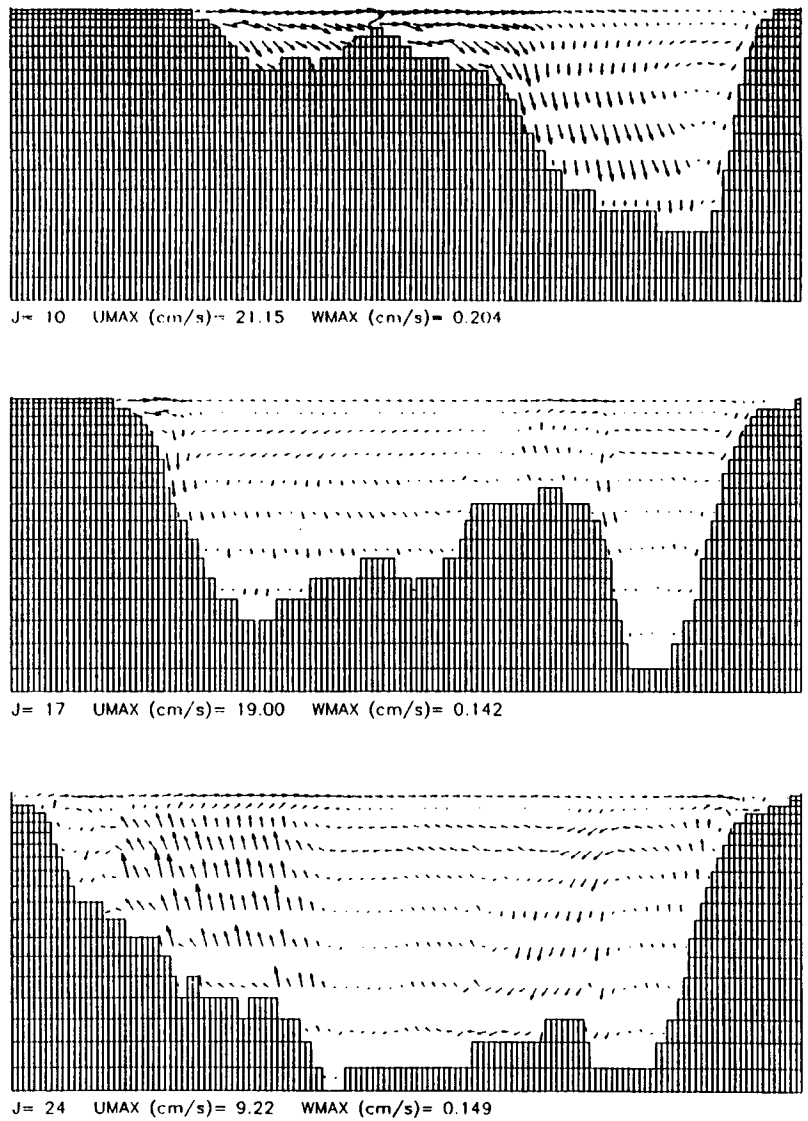

Figure 4. Velocity profiles in 3 longitudinal sections after 12 hours of wind-forcing. "J" increases from south-east to north-west

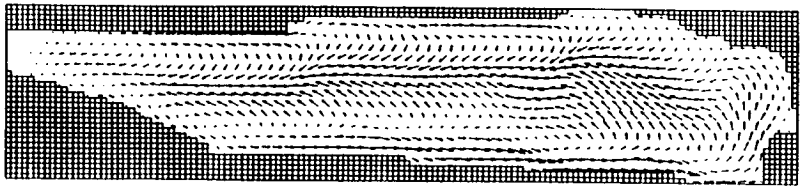

K= 1 Depth (m)= 0.30 VMAX (cm/s)= 12.01

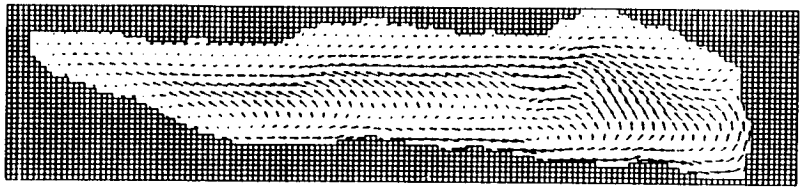

K= 5 Depth (m)= 11.80 VMAX (cm/s)= 9.58

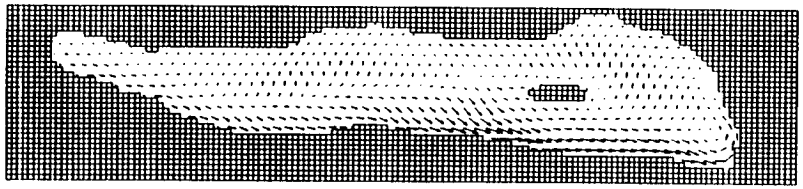

K= 9 Depth (m)= 34.20 VMAX (cm/s)= 7.83

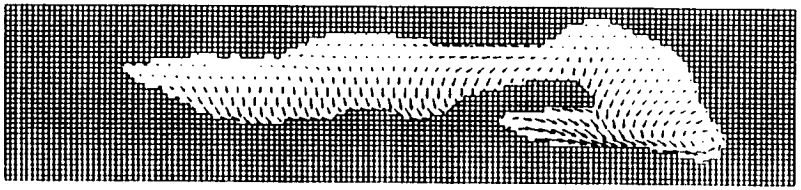

K= 13 Depth (m)= 65.00 VMAX (cm/s)= 4.63

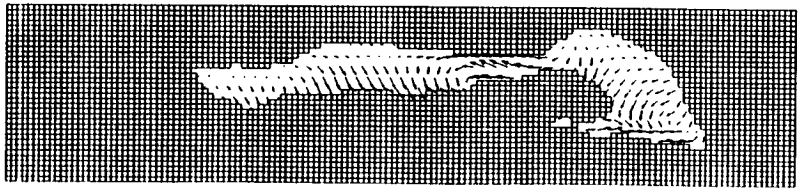

K= 17 Depth (m)= 103.00 VMAX (cm/s)= 1.94

Figure 5. Horizontal velocity field at 5 depth-levels after 18 hours, 6 hours after wind-forcing was stopped

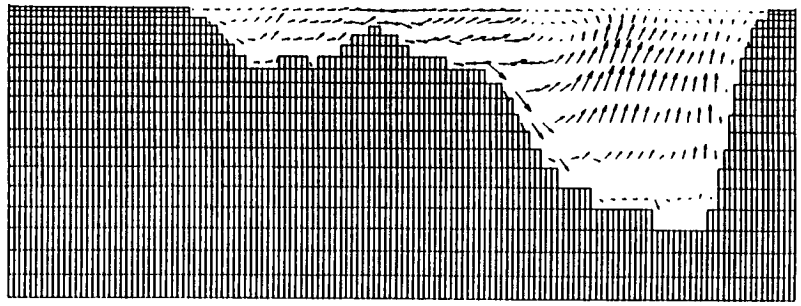

J= 10 UMAX (cm/s)= 8.06 WMAX (cm/s)= 0.115

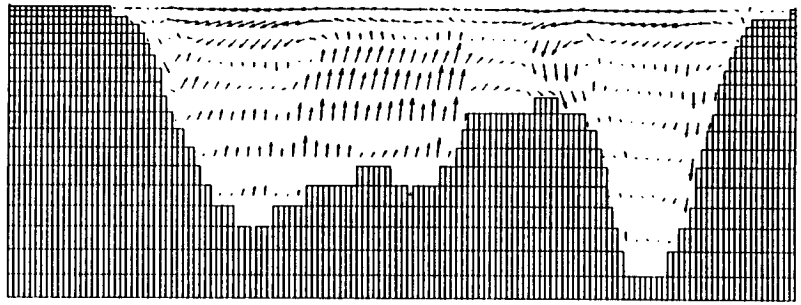

J= 17 UMAX (cm/s)= 6.82 WMAX (cm/s)= 0.098

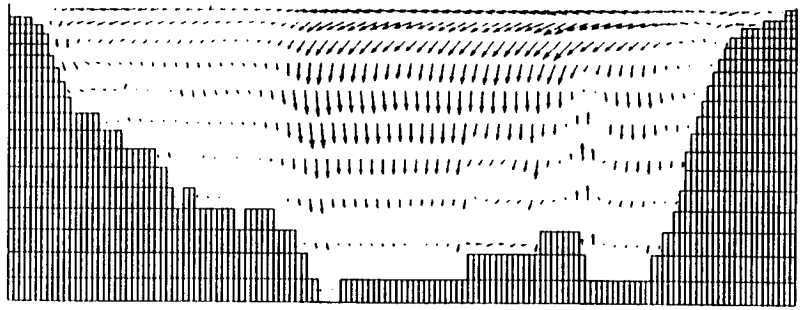

J= 24 UMAX (cm/s)= 8.36 WMAX (cm/s)= 0.093

Figure 6. Velocity profiles in 3 longitudinal sections after 18 hours, 6 hours after wind-forcing was stopped. "J" increases from south-east to north-west

Other parameters used in the calculations have the following values:

- reference density: $\varrho_0 = 1000\ \mathrm{kg/m^3}$;
- Coriolis parameter: $f = 1.05 \times 10^{-4}\ \mathrm{s^{-1}}$;
- gravitational acceleration: $g = 9.8\ \mathrm{m/s^2}$;
- weight coeff. in FLTW method: $\omega = 0.1$;
- time step: $\Delta t = 60\ \mathrm{s}$.

4.3 Results

Results are presented in fig. 3 to fig. 6. For brevity, only 5 among the 20 depth-levels, and 3 among the 34 vertical slices in the length direction of the lake are diplayed. The size of the arrows is scaled according to the maximum velocity that occurs at that level/slice. So, the length of the longest vector at each level/slice is the same, and its magnitude is denoted under the corresponding plot. In the captions of the plots "K" and "J" denote the number of the depth-level and the cross-section respectively. "K" increases from top to bottom from 1 to 20, and "J" increases from south-east to north-west from 1 to 34. Figure 3 and fig. 4 show the situation after 12 hours, fig. 5 and fig. 6 after 18 hours.

After 12 hours of wind forcing the circulation is stationary. Near the surface away from the boundary the velocity-field is deflected to the right relative to the south-west wind (see fig. 3). The angle of this deflection agrees well with the theoretical value, being 45°, which is the limiting angle in the Ekman layer when the surface is approached (Pedlosky, 1986). As the net horizontal flow near the surface is directed east, it induces upwelling in the west- and downwelling in the east-part of the lake (see fig. 4). So, a vortex in the vertical west-east plane has been set up by the wind. After 12 hours the wind is turned off, and the vortex will start to propagate clockwise as to conserve vorticity (apart from the fact that energy is dissipated by eddy viscosity). The strong influence of the pronounced topography on the circulation makes it difficult to identify the mentioned vortex after 18 hours in the plots (see fig. 6). Away from the boundary in the middle of the lake the Coriolis force tends to rotate the velocity field horizontally with inertial period $2\pi/f \simeq 16.6$ hr, while the direction of the currents near the longside boundaries remains unchanged. As a result after 6 hours without wind-forcing two cells are formed in the upper layers, turning in opposite directions (see fig. 5).

5. Conclusions

The favourable stability characteristics of the SOMS model are due to the specific features of the numerical scheme, under which the facts that the mass conservation equation is satisfied in every cell at the end of every timestep, and the finite difference scheme is such that the Coriolis terms conserve energy exactly in the algebraic sense. Compared to explicit "free surface" models, the time step that can be taken in SOMS is much bigger as a result of the rigid lid approximation and the coupled implicit treatment of Coriolis and vertical diffusion.

Some results of applying the model to Lake Neuchâtel under barotropic conditions were presented. The phenomenological magnitudes in the model are the horizontal and vertical turbulent viscosity and the drag coefficients at the surface and bottom. As we had no relevant data available to determine these magnitudes experimentally, we took values which were determined for lakes with comparable dimensions. Since these magnitudes depend particularly on the considered length-scale, this approach is justified. In the near future an extensive field campaign will be carried out in Lake Neuchâtel. With the data that becomes available then, results from modelling the lake's circulation can be verified properly. Then SOMS will also be used to simulate the circulation under baroclinic conditions.

ACKNOWLEDGEMENTS

This research was performed within the framework of a collaboration between the PROSPER group (University of Neuchâtel, Switzerland) and Sandia National Laboratories (New Mexico). It was supported by the Swiss National Science Foundation (grant nr.: 2.055.086). The authors warmly thank Dr. François Nyffeler and Dr. Pat Roache for their contributions and guidance, and Dr. Melvin Marietta who promoted this collaborative effort.

REFERENCES

Arakawa, A., and V. R. Lamb, 1977. Computational design of the basic dynamical processes of the UCLA general circulation model. Methods in Computational Physics. 17:174–265.

Bapst, A., 1987. Le Lac de Neuchâtel: Thèse présentée a la Faculté des Sciences (Université de Neuchâtel).

Batchelor, G. K., 1967. An introduction to fluid dynamics. Cambridge University Press.

Dietrich, D. E., M. G. Marietta and P. J. Roache, 1987. An Ocean Modelling System with turbulent boundary layers and topography. International Journal for Numerical Methods in Fluids. 7:833–855.

Hutter, K., 1984. Mathematische Vorhersage von barotropen und baroklinen Prozessen im Zürich- und Luganersee. Vierteljahrschrift der Naturforschenden Gesellschaft in Zürich. 129:51–92.

Mellor, G. L., and T. Yamada, 1982. Development of a Turbulence Closure Model for Geophysical Fluid Problems. Reviews of geophysics and space physics. 20:851–875.

Pedlosky, J., 1987. Geophysical fluid dynamics. Springer, New York.

Roache, P. J., 1976. Computational Fluid Dynamics. Hermosa Publishers, Albuquerque, New Mexico.

Roache, P. J., and D. E. Dietrich, 1988. Evaluation of the filtered leapfrog-trapezoidal time integration method. Numerical Heat Transfer.

Sollberger, H., 1974. Le Lac de Neuchâtel: Thèse présentée a la Faculté des Sciences (Université de Neuchâtel).

Welch, J. E., F. H. Harlow, J. P. Shannon and B. P. Daly, 1966. The MAC Method, LA-3425. Los Alamos, New Mexico.

Received 20 December 1989;
revised manuscript accepted 16 January 1990.